Supplementary information

Elucidating electrochemical CO_2 reduction reaction processes on Cu(*hkl*) single-crystal surfaces by *in situ* Raman spectroscopy

Yu Zhao,‡[a] Xia-Guang Zhang,‡[b] Nataraju Bodappa,‡[a] Wei-Min Yang,[a] Qian Liang,[a] Petar M. Radjenovica,[a] Yao-Hui Wang,[a] Yue-Jiao Zhang,[ac] Jin-Chao Dong,*[ac] Zhong-Qun Tian[ac] and Jian-Feng Li*[acd]

[a] *State Key Laboratory of Physical Chemistry of Solid Surfaces, iChEM, College of Chemistry and Chemical Engineering, College of Energy, College of Physical Science and Technology, Xiamen University, Xiamen 361005, China.*

[b] *Key Laboratory of Green Chemical Media and Reactions, Ministry of Education, Collaborative Innovation Center of Henan Province for Green Manufacturing of Fine Chemicals, College of Chemistry and Chemical Engineering, Henan Normal University, Xinxiang 453007, China*

[c] *Innovation Laboratory for Sciences and Technologies of Energy Materials of Fujian Province (IKKEM), Xiamen 361005, China.*

[d] *College of Optical and Electronic Technology, China Jiliang University, Hangzhou 310018, China.*

‡ *These authors contributed equally.*

Supplementary Methods

Chemicals

Chloroauric acid ($HAuCl_4$) (99.99%), (3-aminopropyl) trimethoxysilane (APTMS) (97%), sodium citrate (99.0%) and ethylene glycol (>99.0%) were purchased from Alfa-Aesar; H_2SO_4 (95%), H_3PO_4 (85%), and Acetic acid (99%) were purchased from Sinopharmsodium; silicate solution (27% SiO_2) were purchased from Sigma-Aldrich. potassium hydroxide (99.99%) was purchased from Aladdin. $KHCO_3$ (≥ 99.99%), KOH (99.99%) were purchased from Aladdin. $KClO_4$ (99.9%) and D_2O (for NMR atom % 99.9 D) were purchased from Innochem. Argon (99.999%), $^{12}CO_2$ (99.99%), $^{13}CO_2$, and ^{12}CO (99.9%) was purchased from Linde. CO_2 saturated $KHCO_3$ electrolyte was prepared by purging CO_2 into KOH for 20 min. Milli Q water (18.2 MΩ.cm) was used throughout the experiment.

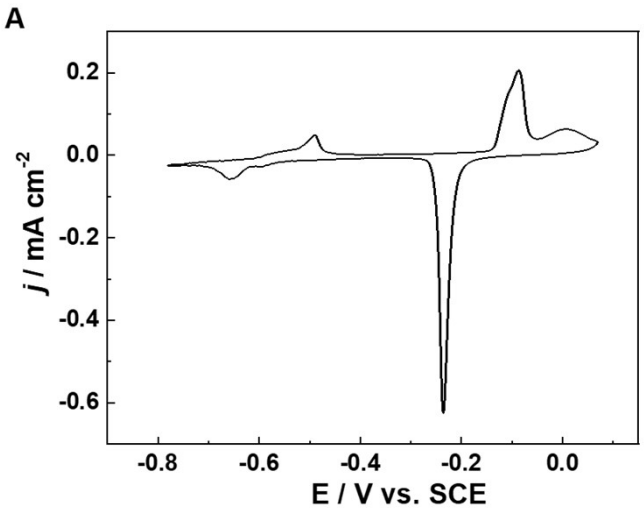

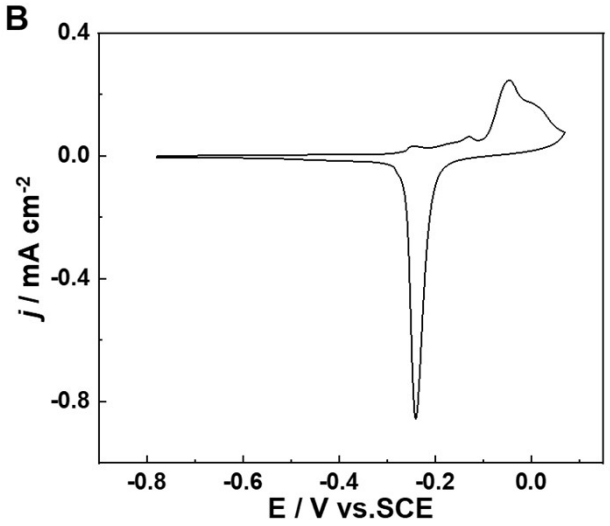

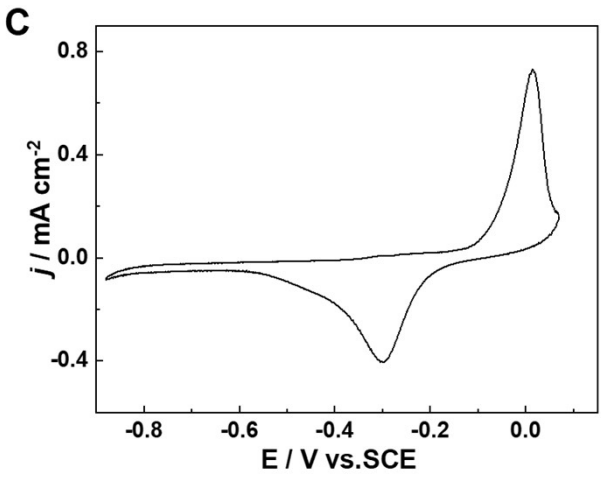

Fig. S1. Electrochemical characterization of Cu(*hkl*) and Cu(poly) electrodes. CVs of Cu(111) (**A**), Cu(110) (**B**) single crystals and Cu(poly) (**C**) surfaces in 0.1 M KOH saturated with argon, ν = 0.05 V s^{-1}.

The electrochemical behaviors of Cu(111), Cu(110) and Cu(poly) were tested by CV in 0.1 M KOH solution (**Fig. S1**). Compared with the literature[1], it was determined that the properties of the single crystal used in the experiment were relatively intact.

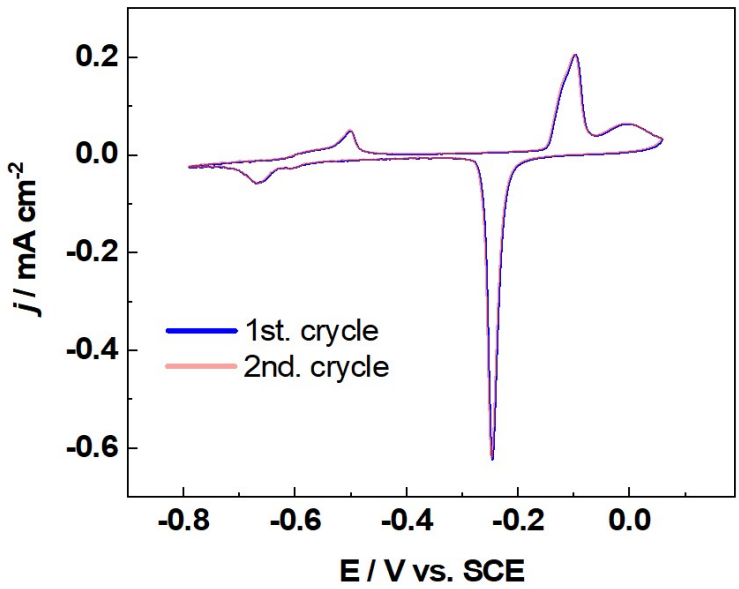

Fig. S2. Investigation on the stability of Cu(111) surface structure. First and second cycles of CV of Cu(111) single crystal surfaces in 0.1 M KOH saturated with argon, $\nu = 0.05$ V s^{-1}.

The electrochemical behavior of the first and second cycles of Cu(111) surface in0.1 M KOH solution is consistent, which proves that the performance of Cu(111) can be maintained after the redox process.

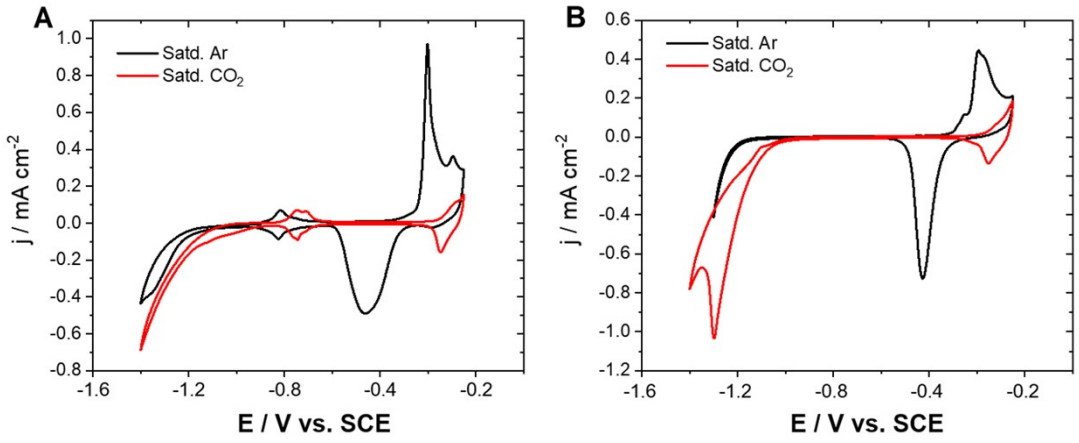

Fig. S3. The control experiment of Cu(*hkl*) in argon and CO_2 atmosphere, respectively. CVs of (A) Cu(111) and (B) Cu(110) in 0.1 M $KHCO_3$ saturated with Ar (black curve) and saturated with CO_2 (red curve), $\nu = 0.05$ V s^{-1}.

In **Fig. S3**, we found that the electrochemical peak of Cu-oxygen species on the Cu(*hkl*) surface

at -0.4 V was obviously suppressed by the presence of CO_2 in the 0.1 M $KHCO_3$ solution (sat. Ar), indicating that CO_2 was adsorbed on the Cu(*hkl*) surface at this potential.

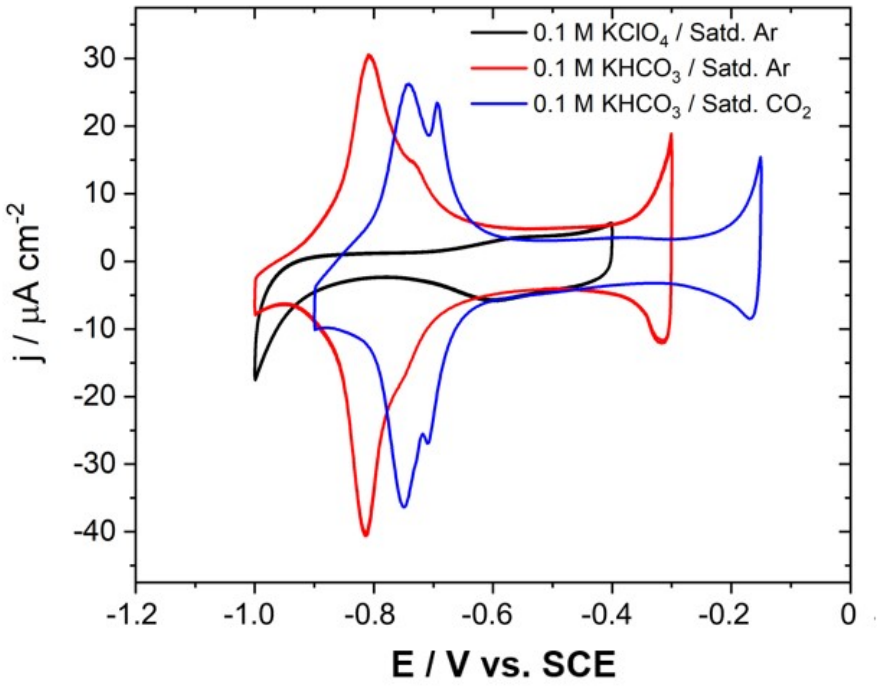

Fig. S4. CVs of Cu(111) in different solution. CVs of Cu(111) in 0.1 M $KClO_4$ saturated with Ar (black curve), 0.1 M $KHCO_3$ saturated with Ar (red curve) and 0.1 M $KHCO_3$ saturated with CO_2 (blue curve), $\nu = 0.05$ V s^{-1}.

Control CVs of Cu(111) were carried out in different solutions as shown in **Fig. S4**, the broad CV feature peak around -0.8 V remains the same in Ar sat. 0.1 M $KHCO_3$, but this feature was absent in Ar sat. 0.1 M $KClO_4$ solution. These results reveal that the peaks around -0.8 V should arise from the HCO_3^-or CO_2 interaction with the Cu(111) surface.

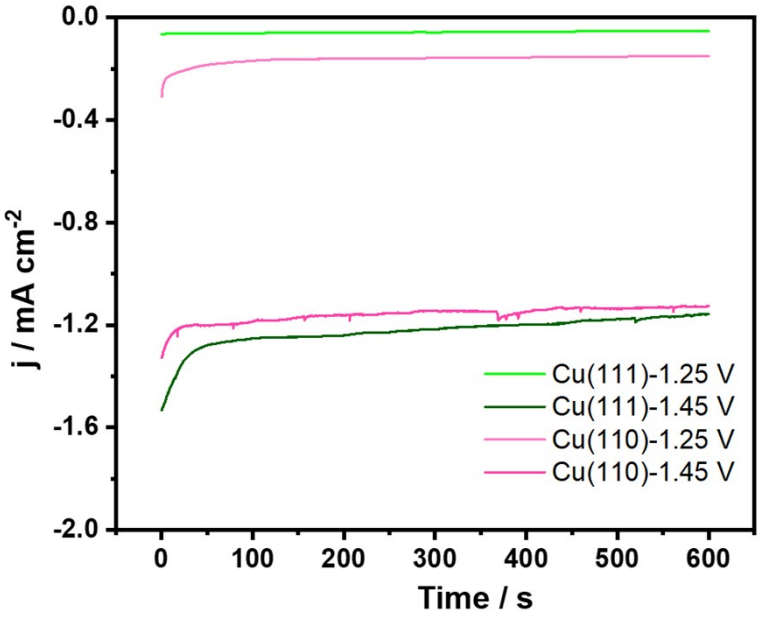

Fig. S5. i-t curves of Cu(111) and Cu(110) Chronoamperometric curves of Cu(111) and Cu(110) single crystals at various potentials.

In situ Raman of CO_2RR on the Cu(hkl) and Spectral peak attribution

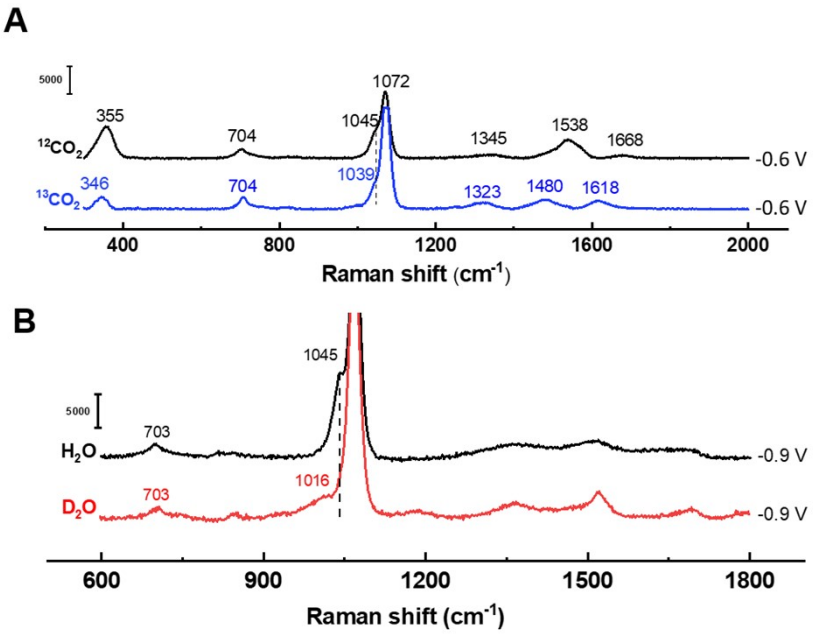

Fig. S6. The isotope experiments of *CO_2^- and *COOH species. Comparison of *in situ* SERS spectra of CO_2RR on Cu(poly) at -0.6 V(**a**) and -0.9 V(**b**) in 0.5 M $KHCO_3$/satd. CO_2 (black curve); 0.5 M $NaH^{13}CO_3$/bubbling $^{13}CO_2$ (blue curve); 0.5 M K_2CO_3/CO_2/D_2O (red curve).

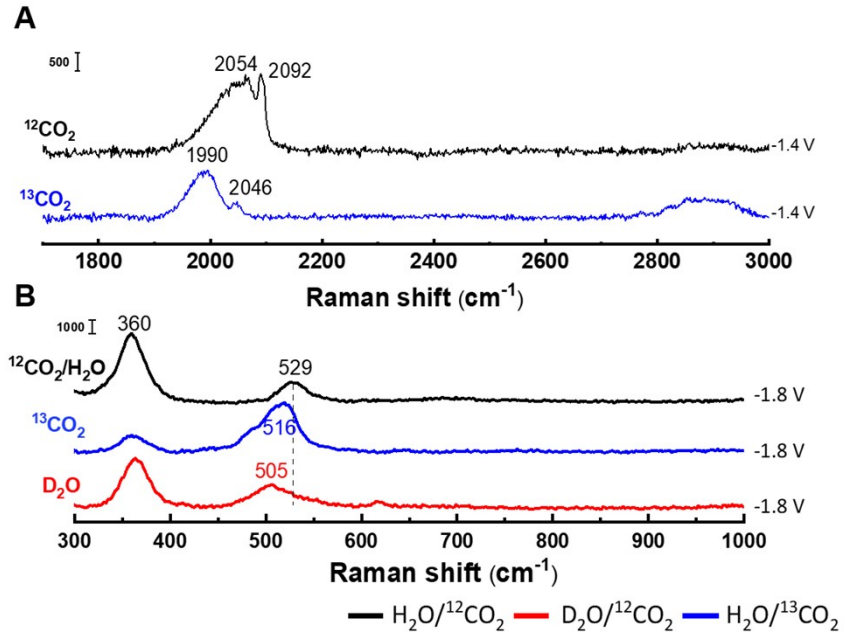

Fig. S7. The isotope experiments of *CO, *OCCO and *CH_2CHO species. comparison of *in situ* SERS spectra of CO_2RR on Cu(poly) at -1.4 V(**A**) and -1.8 V(**B**) in 0.5 M $KHCO_3$/sat. CO_2 (black curve); 0.5 M $NaH^{13}CO_3$ bubbling $^{13}CO_2$ (blue curve); 0.5 M K_2CO_3/CO_2/D_2O (red curve).

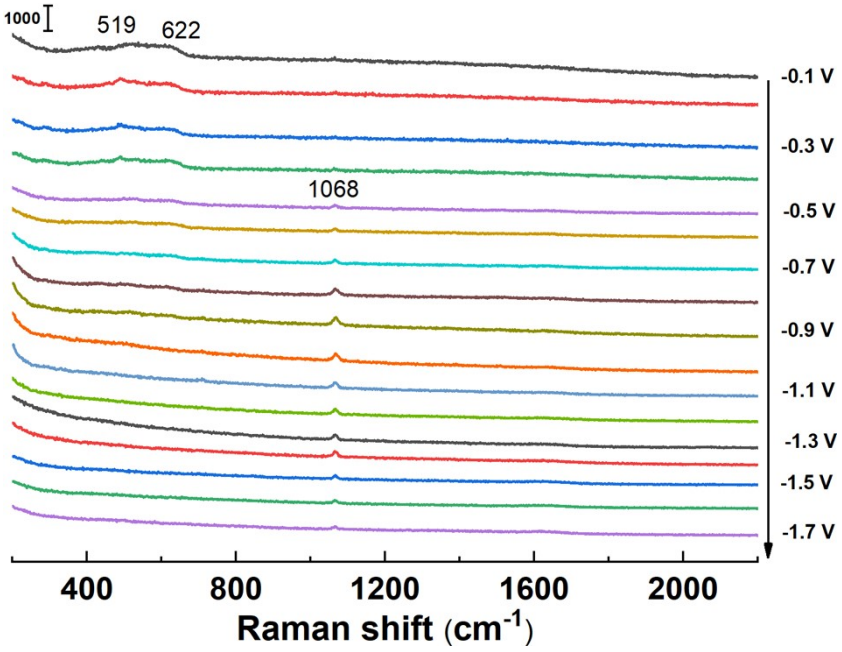

Fig. S8. The control experiment of K_2CO_3 solution. In situ SERS spectra of Cu(poly) in 0.8 M K_2CO_3 solution without CO_2.

To investigate the adsorption of CO_3^{2-} on the copper electrode surface, we investigated the electrochemical process of the Cu electrode surface in 0.8 M K_2CO_3 solution (Fig. S8). Except for the Raman peaks of Cu_2O around 519 cm^{-1} and 622 cm^{-1} and the Raman peak of CO_3^{2-} at 1068 cm^{-1} appeared, no other obvious Raman peak around 1554 cm^{-1} was observed.

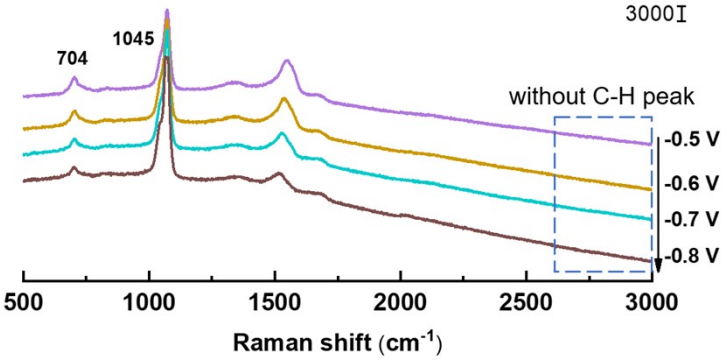

Fig. S9. The low and high wavenumber spectral of CO_2RR on Cu(poly) surface. *In situ* SERS of Cu(poly) in 0.5 M $KHCO_3$ solution sat. CO_2.

The in-situ Raman spectral results of CO_2RR on the Cu(poly) electrode surface show that no obvious C-H stretching vibration peak information is observed at high wavenumber (Fig. S9), which indicates that the 1045 cm^{-1} peak should not be attributed to the HCOO species.

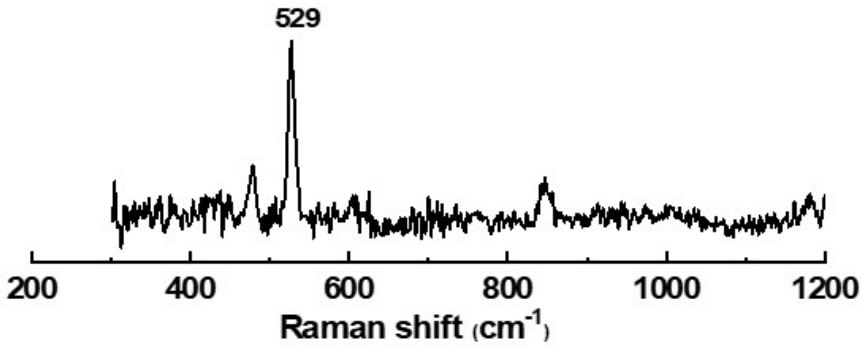

Fig. S10. The Raman spectra of CH_3CHO. Raman spectra of 10% acetaldehyde acid sample.

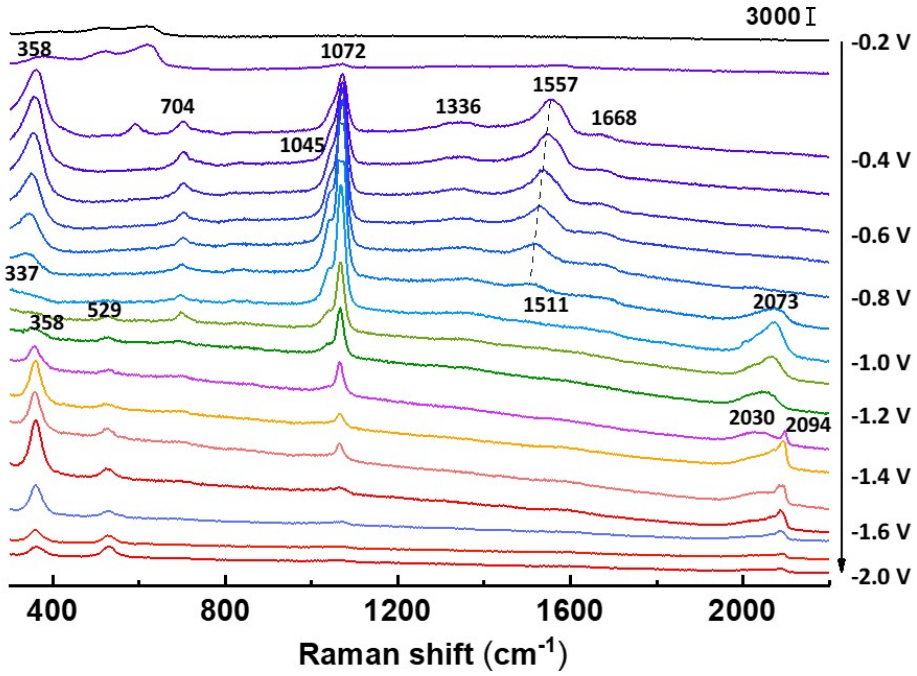

Fig. S11. In situ Raman spectra of CO_2RR reaction on Cu(poly). *In situ* SERS spectra of Cu(poly) in 0.5 M $KHCO_3$ saturated with CO_2. pH = 6.8 (*vs*. SCE).

In order to accurately identify the attribution of the spectral Raman peaks of the CO_2RR-related intermediate species, and the results on Cu (poly) are similar to those on Cu(110) surface(Fig. S11), we conducted a systematic isotope substitution experiment on Cu (poly) surface during the CO_2RR

process. To compare the offset of relative Raman peak in ^{13}C and D_2O experiments more accurately, we have selected different potentials for comparison as shown in Fig. S5-6. We found that the peak ~355 cm^{-1} shifts to around 346 cm^{-1} in ^{13}C experiment. Thus, this peak should be correlated with the "C" atom. The peak ~1045 cm^{-1} shifts to around 1039 cm^{-1} and 1016 cm^{-1} in ^{13}C and D_2O experiments, respectively. So Thus, this peak should be correlated with "C" and "H" atoms. The peak of 1345 cm^{-1}, 1538 cm^{-1} and 1668 cm^{-1} shift to lower wavenumber around 1323 cm^{-1}, 1480 cm^{-1} and 1618 cm^{-1} in $^{13}CO_2$, respectively. The peak of 2054 cm^{-1} and 2092 cm^{-1} shift to 1990 cm^{-1} and 2046 cm^{-1} respectively. The peak of 529 cm^{-1} shift to lower wavenumber in both D_2O and $^{13}CO_2$.

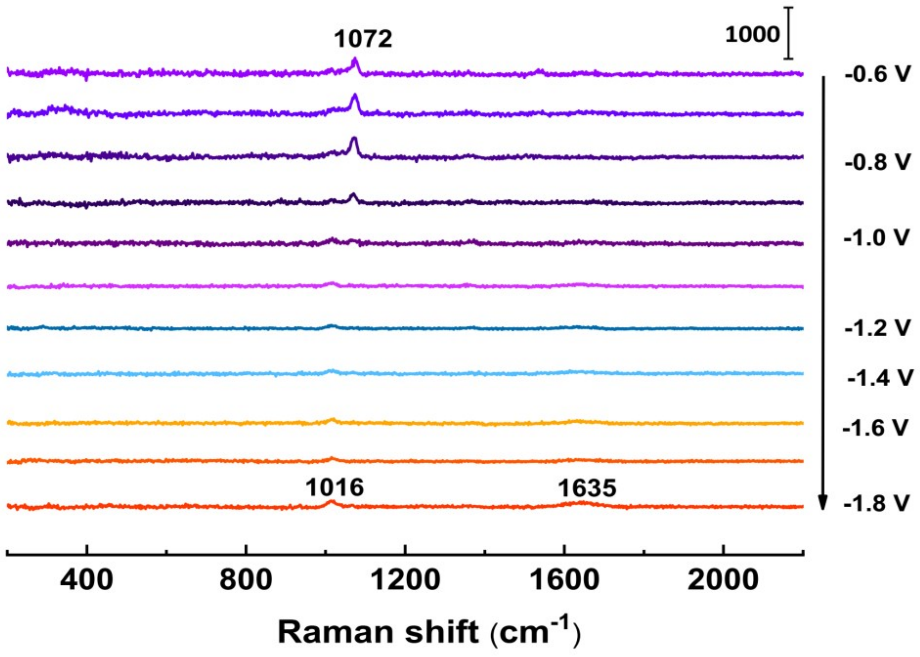

Fig. S12. In situ Raman spectra of CO_2RR process on Cu surface. In situ Raman spectra of Cu(poly) in 0.5 M $KHCO_3/H_2O$ (sat. CO_2) without Cu_2O in the initial potential.

After we first reduce the Cu(poly) electrode at very negative potential and then conduct *in situ* Raman study of the CO_2RR from -0.6 V (Fig. S12), no other characteristic Raman peaks appeared except for the Raman peaks of HCO_3^- and CO_3^{2-} around 1016 cm^{-1} and 1072 cm^{-1}, indicating that the presence of Cu_2O or Cu oxides in the initial potential range has an important effect for activating

CO_2 during the CO_2RR process.

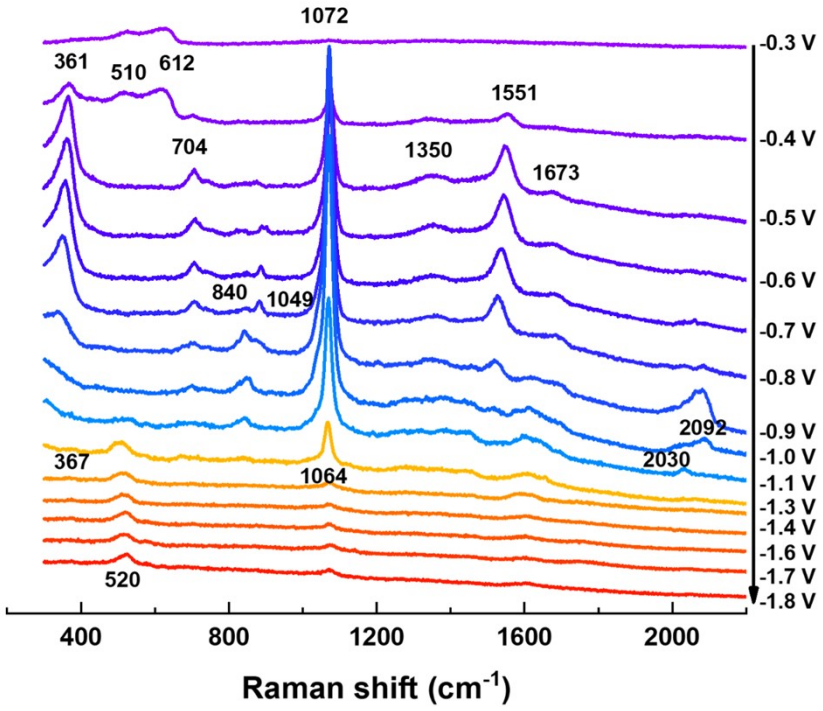

Fig. S13 *In situ* Raman spectra of CO_2RR reaction on Cu(100). *In situ* SHINERS of Cu(100) in 0.5 M $KHCO_3$ saturated with CO_2. pH = 6.8 (*vs*. SCE).

Detection of CO_2RR liquids products

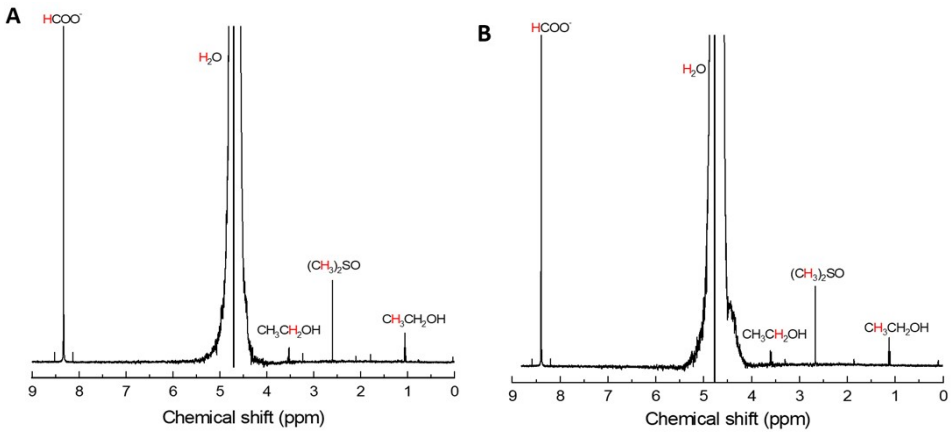

Fig. S14. NMR for liquid product analysis. ^{1}H NMR spectrum obtained on the Cu(111) (**A**), Cu(110) (**B**) electrode at -1.65 V in 0.5 M $KHCO_3$ CO_2 saturated for liquid product analysis. DMSO and phenol were added as internal standards.

The concentration effect of $KHCO_3$

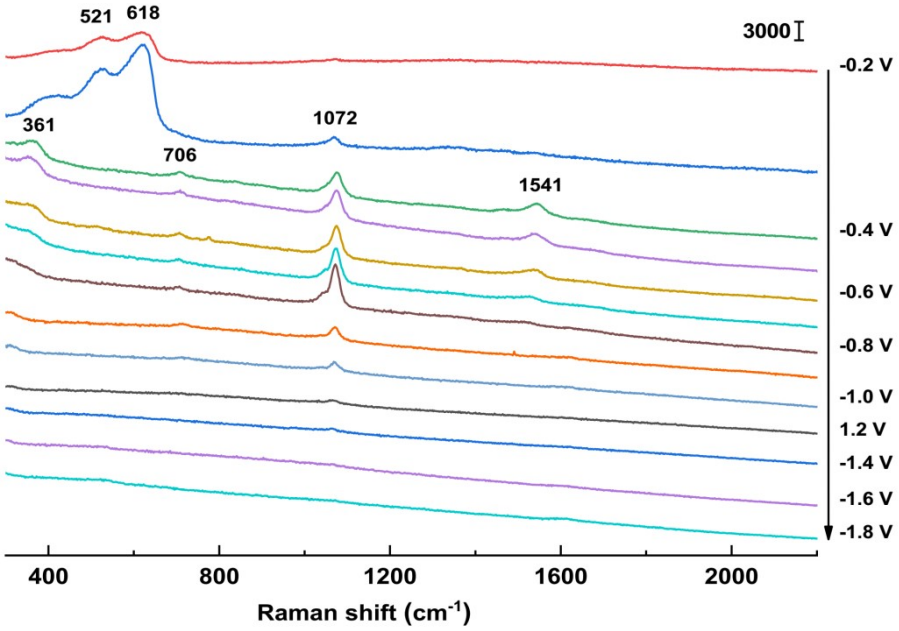

Fig. S15. *In situ* Raman spectra of Cu(poly) in 0.2 M $KHCO_3$. *In situ* SERS spectra of Cu(poly) in 0.2 M $KHCO_3/H_2O$ without CO_2 gas.

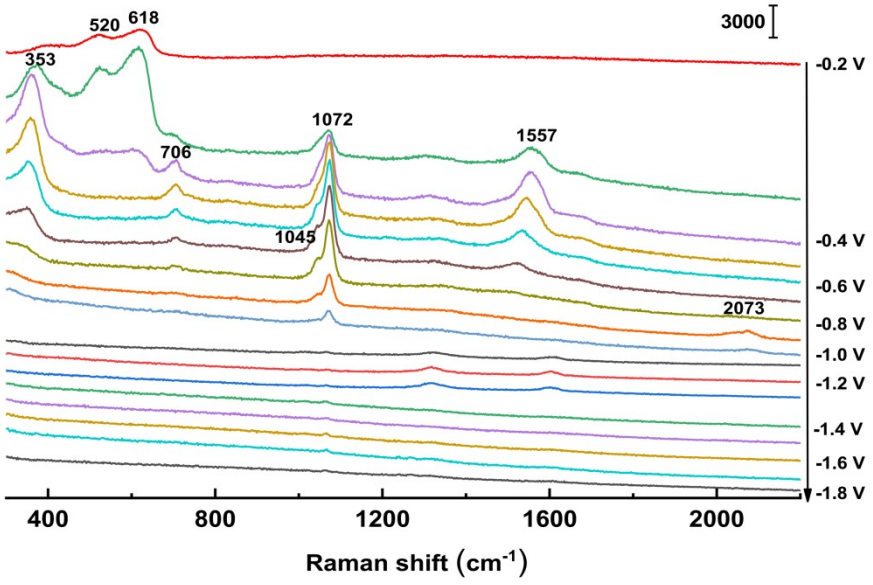

Fig. S16. In situ Raman spectra of Cu(poly) in 0.3 M $KHCO_3$. In situ SERS spectra of Cu(poly) in 0.3 M $KHCO_3/H_2O$ without CO_2 gas.

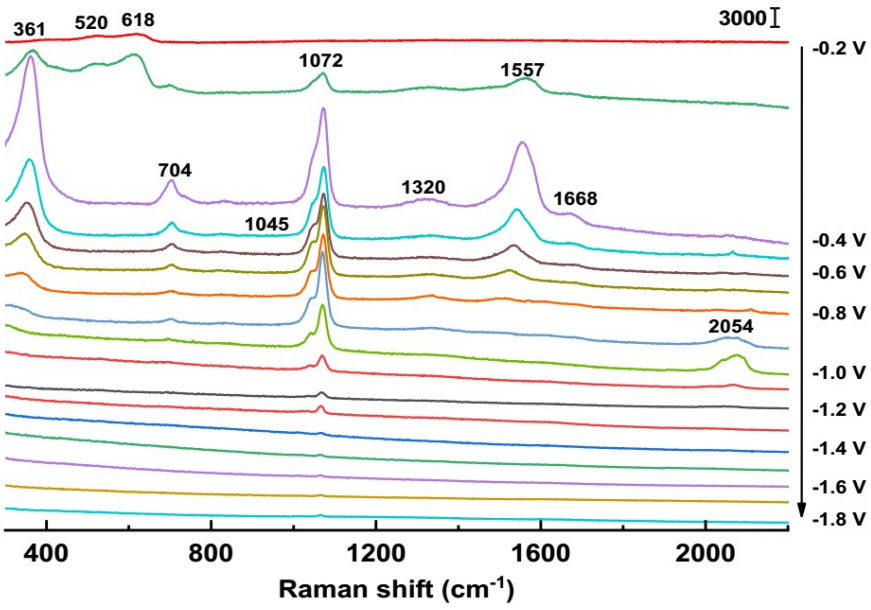

Fig. S17. In situ Raman spectra of Cu(poly) in 0.4 M $KHCO_3$. In situ SERS spectra of Cu(poly) in 0.4 M $KHCO_3/H_2O$ without CO_2 gas.

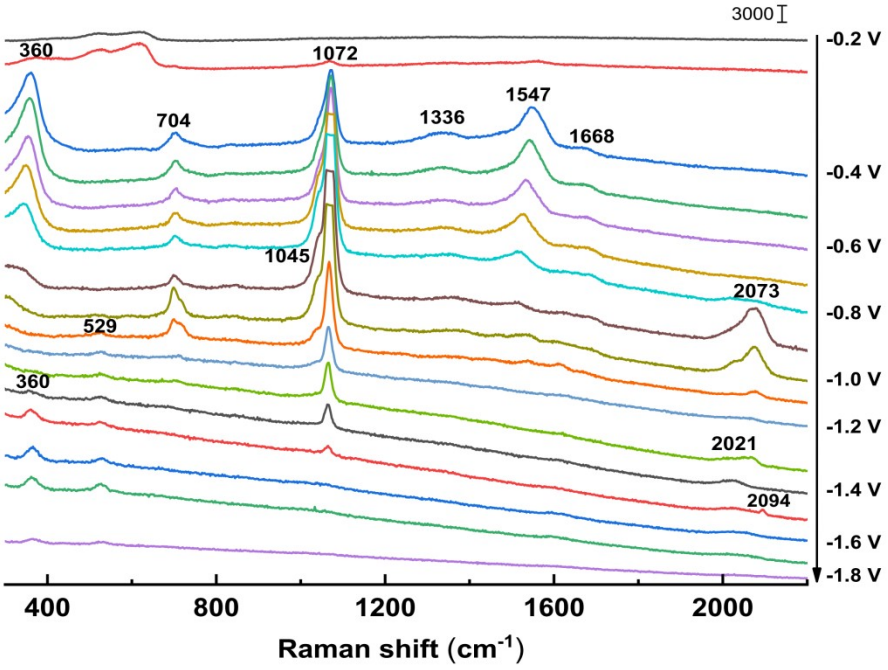

Fig. S18. In situ Raman spectra of Cu(poly) in 0.6 M $KHCO_3$. In situ SERS spectra of Cu(poly) in 0.6 M $KHCO_3/H_2O$ without CO_2 gas.

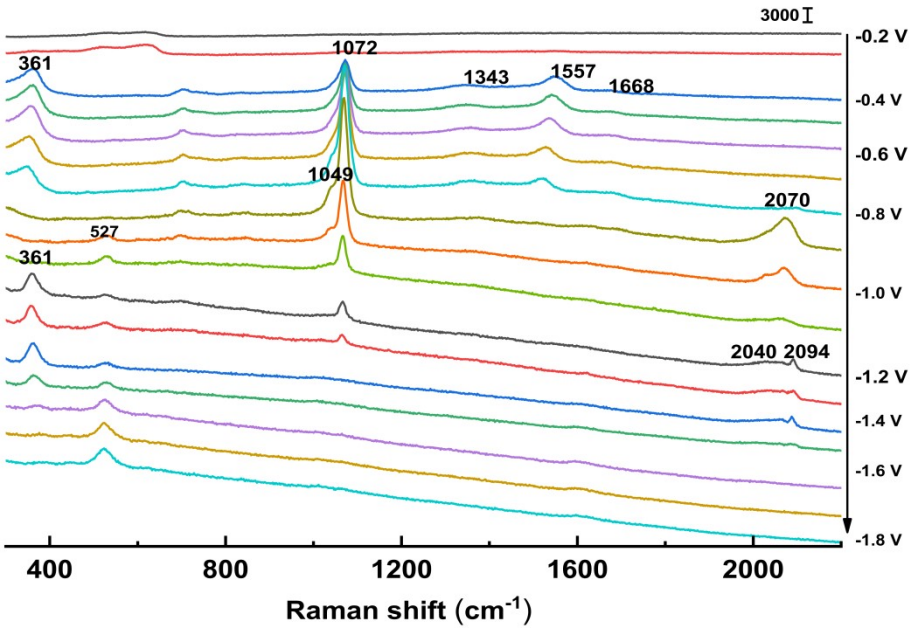

Fig. S19. In situ Raman spectra of Cu(poly) in 0.8 M $KHCO_3$. In situ SERS spectra of Cu(poly) in 0.8 M $KHCO_3/H_2O$ without CO_2 gas.

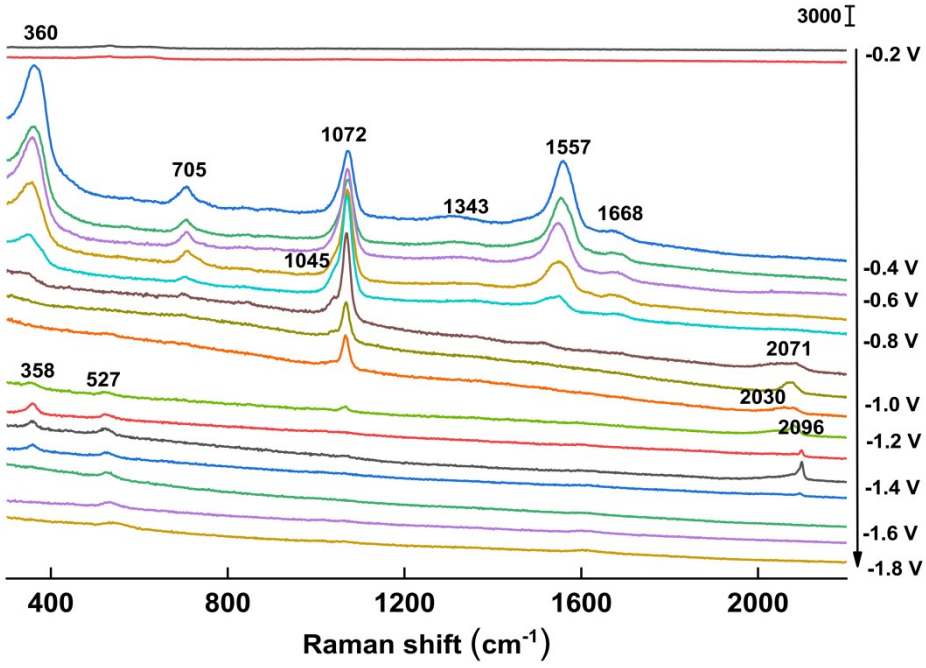

Fig. S20. In situ Raman spectra of Cu(poly) in 1.0 M $KHCO_3$. In situ SERS spectra of Cu(poly) in 1.0 M $KHCO_3/H_2O$ without CO_2 gas.

Results of different concentrations of $KHCO_3$ on Cu(poly) surface. In order to investigate the

concentration effect of the $KHCO_3$ electrolyte, we have investigated the reaction process of Cu (poly) surface under different concentration conditions. As the concentration increases, we found that the characteristic Raman peaks of CO_2RR-related intermediate species gradually become apparent. (Fig. S15-S20)

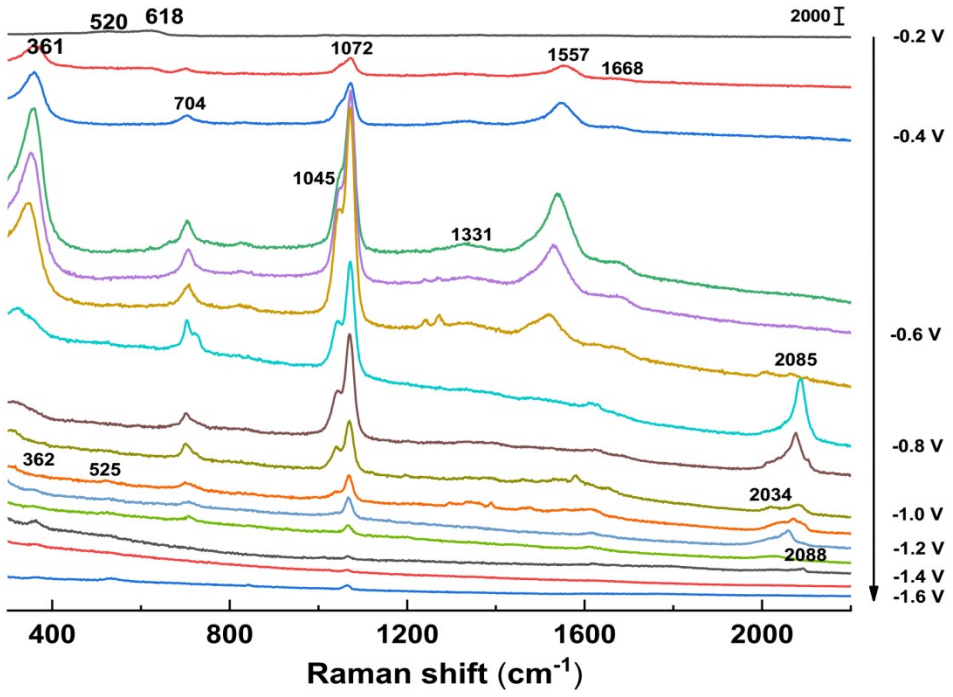

Fig. S21. In situ Raman spectra of Cu(poly) in 0.4 M $KHCO_3$ solution CO_2-saturated. In situ SERS spectra of Cu(poly) in 0.4 M $KHCO_3/H_2O$ with CO_2 gas.

After introduced CO_2 gas into the 0.4 M $KHCO_3$ solution, we found that the peaks of CO_2RR related intermediate species became more obvious, and the characteristic peaks of *OCCO (2088 cm^{-1}) and *CH_2CHO (525 cm^{-1}) appeared in low potential range.

Computational results:

In this study, different adsorption structures of CO_2RR intermediates which adsorbs at Cu(*hkl*) surface have been calculated as following.

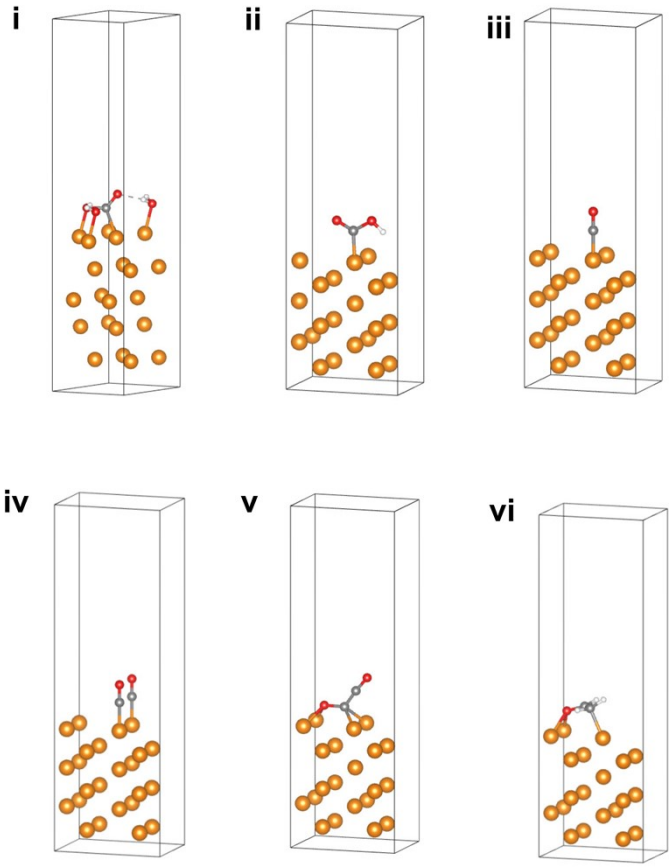

Fig. S22. The model of different intermediates at Cu(110) crystal facet. The side view of **(i)***CO_2^-; **(ii)***COOH; (**iii**)*CO; **(iv)** *CO-*CO; **(v)** *OCCO and **(vi)** *CH_2CHO.

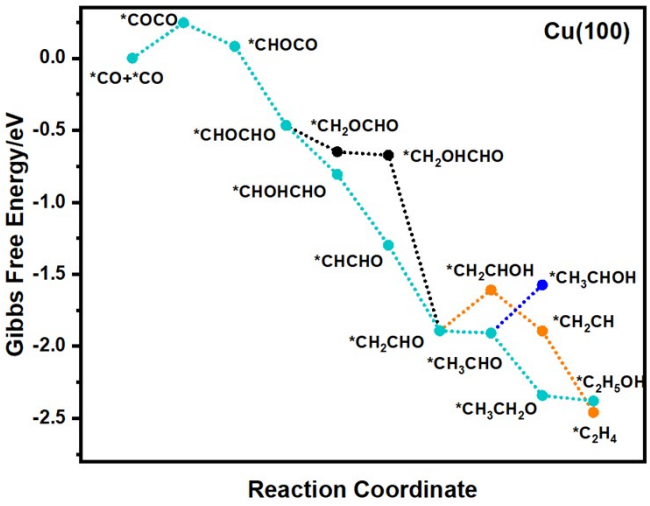

Fig. S23. The possible mechanism of CO_2RR on Cu(100). The possible mechanism of CO_2RR mechanism to CH_4 on Cu(100) surface and relevant Gibbs free energy of different intermediates.

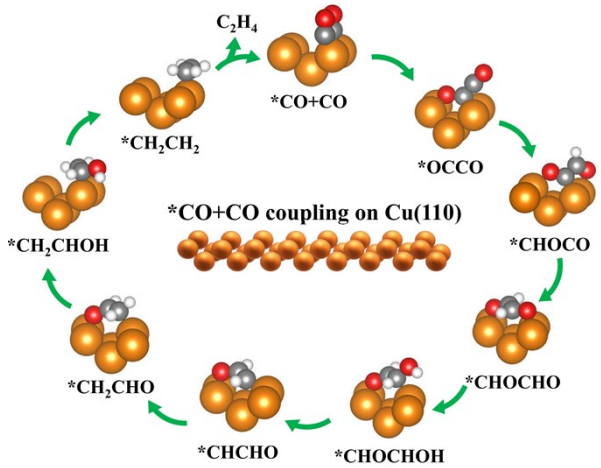

Fig. S24. The possible mechanism of *CO coupling to produce C_2 product on Cu(110). The possible mechanism of CO_2RR mechanism to C_2H_4 on Cu(110) surface.

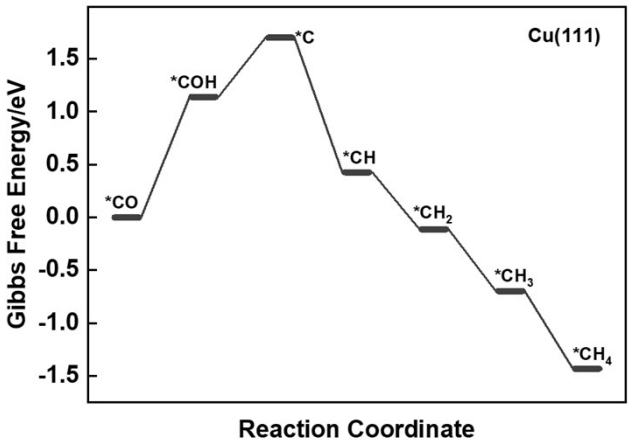

Fig. S25. The possible mechanism of CO_2RR on Cu(111). The possible mechanism of CO_2RR mechanism to CH_4 on Cu(111) surface and relevant Gibbs free energy of different intermediates.

Table 1. Vibrational frequencies of stable intermediates on Cu(110) surface.

	$^{12}CO_2/H_2O$	$^{12}CO_2/D_2O$	$^{13}CO_2/H_2O$
$*CO_2$	1698/1527/698	1669/1157/711	1665/1519/688
$*CO_2H$	1039/1705	1058/1698	1017/1696
*COCO	2051	-	1992
$*CH_2CHO$	519	444	513
*CO	2029	-	1982
Two *CO	2067/1986	-	2019/1941

Table 2. Vibrational frequencies of stable intermediates on Cu(100) surface.

	$^{12}CO_2/H_2O$	$^{12}CO_2/D_2O$	$^{13}CO_2/H_2O$
$*CO_2H$	1482/1220/1150	1458/1188/904	1448/1209/1132
*COCO	2090	-	2031
$*CH_2CHO$	516	447	511
*CO	2027	-	1981
Two *CO	2066/1977	-	2019/1933

Table 3. Simulation parameters of Gibbs free energy calculated for CO_2RR on Cu(110)

surface (eV)

species	E_{DFT}	E_{ZPE}	$\int C_v dT$	TS	G
Cu(110)	-90.546				
*CO-CO	-121.560	0.406	0.116	0.222	-121.260
*OCCO	-121.344	0.409	0.123	0.245	-121.057
*CHOCO	-125.294	0.703	0.124	0.234	-124.701
*CHOCHO	-129.643	0.998	0.129	0.249	-128.765
*CH_2OCHO	-133.284	1.271	0.141	0.259	-132.131
*CH_2OHCHO	-136.959	1.630	0.138	0.250	-135.441
*CHOHCHO	-133.470	1.321	0.145	0.283	-132.287
*CHCHO	-121.919	0.877	0.098	0.176	-121.120
*CH_2CHO	-127.084	1.212	0.108	0.202	-125.966
*CH_2CHOH	-130.272	1.500	0.133	0.289	-128.928
*CH_3CHO	-130.345	1.474	0.152	0.340	-129.059
*CH_3CHOH	-133.816	1.809	0.133	0.253	-132.127
*CH_2CH	-119.049	1.078	0.084	0.157	-118.044
*C_2H_5OH	-138.310	2.139	0.160	0.373	-136.384
*C_2H_4	-123.522	1.401	0.101	0.223	-122.243

Table 4. Simulation parameters of Gibbs free energy calculated for CO_2RR on Cu(100)

surface (eV)

species	E_{DFT}	E_{ZPE}	$\int C_v dT$	TS	G
Cu(100)	-94.229				
*CO-CO	-125.086	0.389	0.096	0.177	-124.769
*OCCO	-124.827	0.418	0.119	0.234	-124.524
*CHOCO	-128.652	0.680	0.137	0.269	-128.104
*CHOCHO	-132.968	1.010	0.123	0.235	-132.070

*CH_2OCHO	-136.829	1.309	0.145	0.295	-135.670
*CH_2OHCHO	-140.665	1.658	0.127	0.230	-139.110
*CHOHCHO	-137.038	1.337	0.138	0.263	-135.826
*CHCHO	-126.124	0.924	0.093	0.167	-125.274
*CH_2CHO	-130.398	1.207	0.110	0.205	-129.286
*CH_2CHOH	-133.776	1.508	0.134	0.285	-132.419
*CH_3CHO	-133.972	1.465	0.140	0.351	-132.718
*CH_3CHOH	-137.458	1.803	0.141	0.287	-135.801
*CH_2CH	-122.659	1.077	0.088	0.167	-121.661
*C_2H_5OH	-141.958	2.133	0.160	0.358	-140.023
*C_2H_4	-126.911	1.391	0.107	0.229	-125.642

Table 5. Simulation parameters of Gibbs free energy calculated for CO_2RR on Cu(111) surface (eV)

species	E_{DFT}	E_{ZPE}	$\int C_v dT$	TS	G
Cu(111)	-95.458				
COH	-113.864	0.465	0.083	0.156	-113.472
C	-101.955	0.093	0.018	0.026	-101.870
CH	-106.898	0.352	0.030	0.042	-106.558
CH_2	-111.054	0.581	0.062	0.103	-110.514
CH_3	-115.335	0.909	0.063	0.153	-114.516
CH_4	-119.769	1.194	0.063	0.154	-118.666

Supplementary References

(1) Klaas Jan P. Schouten, Elena Pérez Gallent & Marc T.M. Koper. (2013). The electrochemical characterization of copper single-crystal electrodes in alkaline media. *J. Electroanal. Chem.* 699, 6-9.